JACS
JOURNAL OF THE AMERICAN CHEMICAL SOCIETY

ARTICLE

pubs.acs.org/JACS

Differentiation of O−H and C−H Bond Scission Mechanisms of Ethylene Glycol on Pt and Ni/Pt Using Theory and Isotopic Labeling Experiments

Michael Salciccioli, Weiting Yu, Mark A. Barteau, Jingguang G. Chen,* and Dionisios G. Vlachos*

Department of Chemical Engineering, Catalysis Center for Energy Innovation and Center for Catalytic Science and Technology, University of Delaware, Newark, Delaware 19716-3110, United States

Supporting Information

ABSTRACT: Understanding and controlling bond-breaking sequences of oxygenates on transition metal catalysts can greatly impact the utilization of biomass feedstocks for fuels and chemicals. The decomposition of ethylene glycol, as the simplest representative of biomass-derived polyols, was studied via density functional theory (DFT) calculations to identify the differences in reaction pathways between Pt and the more active Ni/Pt bimetallic catalyst. Comparison of the computed transition states indicated three potentially feasible paths from ethylene glycol to C1 oxygenated adsorbates on Pt. While not important on Pt, the pathway to 1,2-dioxyethylene (OCH_2CH_2O) is favored energetically on the Ni/Pt catalyst. Temperature-programmed desorption (TPD) experiments were conducted with deuterated ethylene glycols for comparison with DFT results. These experiments confirmed that decomposition of ethylene glycol on Pt proceeds via initial O−H bond cleavage, followed by C−H and the second O−H bond cleavages, whereas on the Ni/Pt surface, both O−H bonds are cleaved initially. The results are consistent with vibrational spectra and indicate that tuning of the catalyst surface can selectively control bond breaking. Finally, the significant mechanistic differences in decomposition of polyols compared to that of monoalcohols and hydrocarbons serve to identify general trends in bond scission sequences.

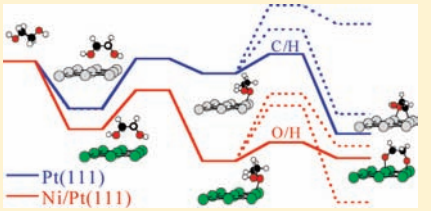

1. INTRODUCTION

The chemistry of oxygenates on transition metal catalysts has garnered interest recently due to the global shift toward utilizing renewable biomass for energy and value-added chemical production. Smaller oxygenates, specifically ethylene glycol ($C_2H_6O_2$), have been used as biomass surrogates to probe catalytic activity and selectivity for larger polyols and sugars.[1,2] Oxygenates with a 1:1 ratio of carbon to oxygen are particularly attractive because, unlike less oxygenated molecules, they do not require (at least in principle) the addition of steam or oxygen to remove carbon from the metal in reforming processes.[3] Ethylene glycol is the smallest oxygenate of this type to contain the C−H, O−H, C−C, and C−O bonds that are present in biomass. Further, ethylene glycol can be directly obtained catalytically from cellulose with high selectivity.[4] As a result, it is an interesting surrogate compound for biomass processing. Platinum (Pt) has been specifically identified as a promising catalyst for oxygenate conversion because of its combination of high reforming activity, synthesis gas product selectivity, and water−gas shift activity.[5] The Ni/Pt bimetallic surface (which is composed of a Pt catalyst with a single monolayer of nickel deposited on the surface) has been shown to exhibit higher activity for oxygenate decomposition compared to Pt, but the origin of this enhanced activity remains elusive.[1,3,6−10] Understanding of such phenomena is needed to improve our ability to tune catalysts for increased activity and selectivity.

While experimental studies on supported metal catalysts[2,11] and on a metal in ultrahigh vacuum (UHV) conditions[1,3,8,9,12,13] have provided some insights into ethylene glycol-reforming pathways, the kinetics of catalytic decomposition are still not well understood. Understanding the bond-breaking sequence is essential. Over the past several years, the decomposition of the smallest oxygenate with a 1:1 carbon to oxygen ratio, methanol, has been extensively studied on Pt(111) using density functional theory (DFT).[14−16] A key element missing from methanol chemistry is the carbon−carbon bond scission. Ultimately, the product selectivity of a metal catalyst for reforming of higher oxygenates is a result of carbon−carbon bond-cleaving activity compared to carbon−oxygen bond-cleaving activity.[17] Further, it has been shown that C−C bond-cleaving reactions are rate determining in hydrocarbon decomposition chemistries.[18−21] Similarly, experimental studies have shown that C−C bond-cleaving rates are slower than dehydrogenation reactions for ethanol at temperatures near 500 K on Pt.[22] While DFT studies of ethanol on Pt(111) have shown that rate constants for C−C bond cleavage are higher than those for ethane due to oxygen destabilization,[23] it is unclear whether C−C bond cleavage is kinetically limiting for decomposition of more highly oxygenated species, such as ethylene glycol.

In this work, we examined the transition states of C−H, O−H, and C−C bond-cleaving reactions for all $C_2H_xO_2$ dehydrogenation intermediates of ethylene glycol via DFT on Pt and select reactions on Ni/Pt. These calculations were validated through

Received: February 27, 2011
Published: April 28, 2011

dx.doi.org/10.1021/ja201801t | J. Am. Chem. Soc. 2011, 133, 7996–8004

temperature-programmed desorption (TPD) experiments with deuterated ethylene glycols ($C_2D_6O_2$, $DOCH_2CH_2OD$ and $HOCD_2CD_2OH$) and comparison with available vibrational spectra. Ethylene glycol lends itself well to these types of experiments because it has a sufficiently high vapor pressure at room temperature to allow for its introduction into ultrahigh vacuum systems with controlled exposure. Additionally, the relative simplicity of ethylene glycol allows for selective deuterium substitution, which is critical in this study to determine the bond scission sequence experimentally. The decomposition pathways on Pt and the more active Ni/Pt bimetallic catalysts were elucidated, along with interesting trends relating energy barriers to intermediate dehydrogenation levels. Finally, these results are compared to previously reported hydrocarbon and alcohol decomposition pathways to identify general trends in bond scission sequences.

2. QUANTUM MECHANICAL CALCULATIONS

All DFT values presented in this work were obtained using the SIESTA code.[24,25] These calculations utilized Troullier−Martins norm-conserving scalar relativistic pseudopotentials,[26] as well as a double-ζ plus polarization (DZP) basis set. An energy shift of 0.01 eV was used to determine the localization radii of the basis functions. A DFT supercell approach with the Perdew−Burke−Ernzerhof (PBE) form of the generalized gradient approximation (GGA) functional[27] was implemented. A mesh cutoff of 200 Ry was used. Systems involving slabs with only Pt atoms utilized the nonspin version of the code, as it has been previously determined that this does not significantly affect the results.[21] Spin polarization is included for calculations on the Ni/Pt(111) surface and for gas-phase species. A four-layered, 3 × 3 unit cell was used for all calculations in this study. The Ni/Pt surface was modeled using three layers of bulk Pt with a top layer of Ni. The surface Monkhorst Pack meshes of 5 × 5 × 1 k-point sampling in the surface Brillouin zone was used in all calculations. The top two layers and the adsorbates were relaxed, while the bottom two layers of Pt were frozen. Details of gas-phase and other intermediate calculations can be found in a previous article.[28] The transition states were identified using a constrained optimization scheme[29−31] whereby the transition state is identified using two requirements: (1) all net forces on atoms approach zero, and (2) the total energy is maximized along the reaction coordinate but minimized with respect to all other degrees of freedom. Vibrational frequency analysis is conducted in order to include zero-point energy (ZPE) corrections on energetic values and to check the existence of a negative frequency mode in the direction of the reaction coordinate for each transition state. The vibrational frequency calculation is based on numerical evaluation of the Hessian matrix for determination of the force constants. Metal atoms were constrained to the original optimization as all atoms of the adsorbate were displaced by 0.015 b in all three Cartesian directions. Diagonalization of the Hessian matrix was followed by subsequent analysis to obtain vibrational frequencies. While C−O bond-cleaving reactions are possible on Pt catalysts,[32] recent studies of ethylene glycol decomposition on Pt and Ni/Pt have shown very little selectivity toward products resulting from C−O bond cleavage.[1] Thus, calculations of C−O bond-cleaving transition states are not included in this study.

The Supporting Information shows images of all optimized DFT structures and gives tabulated vibrational frequencies used for ZPE corrections and information on potential C1 surface intermediates resulting from C−C bond-cleaving reactions. All images in the Supporting Information were created using the Avogadro molecular editor.[33]

3. EXPERIMENTAL METHODS

Isotopes d_2-, d_4-, and d_6-ethylene glycol (Cambridge Isotope Laboratories, Inc., 98%) were transferred into glass sample cylinders and purified using repeated freeze−pump−thaw cycles. All of the other gases used in the experiment, O_2, Ne, and CO, were of research purity and used directly without further purification. The purity of all reagents was verified daily using mass spectrometry.

A UHV chamber was equipped with Auger electron spectroscopy (AES) and a mass spectrometer, a Ni source, and a sputter gun. A Pt(111) single crystal (Princeton Scientific, 99.99%, with 2 mm thickness and 10 mm diameter) was heated using a temperature controller and cooled with liquid nitrogen through two tantalum posts. The temperature was monitored using a chromel−alumel K-type thermocouple spot-welded to the back of the crystal. Procedures for preparing a clean Pt(111) and a monolayer Ni/Pt(111) bimetallic surface were described previously.[7] For all TPD experiments 2 langmuir (L, 1 L = 1 × 10^{-8} Torr × 100 s) of ethylene glycol was dosed at 200 K into the chamber using direct dosing through a 1/4 in. stainless steel tube several inches away from the surface. The TPD experiment was then carried out from a metal surface temperature of 200 K and linearly heating at 3 K/s to 800 K.

4. COMPUTATIONAL RESULTS

4.1. Dehydrogenation of $C_2H_xO_2$ Species. Dehydrogenation reaction transition states for all possible intermediates undergoing sequential dehydrogenation of ethylene glycol without C−C or C−O scission have been calculated. Table 1 contains the energy of each possible transition state relative to that of ethylene glycol in a vacuum, a clean Pt(111) slab and hydrogen adsorbed on separate slabs, the energy change of reaction, and the forward activation energy of the reaction (both in the direction listed in the first column). Table 2 gives the same information for O−H bond-cleaving reactions. Energetic and structural information for all intermediates is contained in the Supporting Information and in our previous publication.[28]

Initial dehydrogenation of ethylene glycol on Pt(111) can proceed through only two unique reactions due to the symmetry of the adsorbate. The transition state for initial O−H scission is 0.22 eV lower than that for initial C−H scission, despite the latter being exothermic. Figure 1 shows the most stable structure of ethylene glycol on Pt(111), along with transition state structures for initial C−H, O−H and C−C bond scission. Table 3 compares the energetics of initial dehydrogenation of alcohols on Pt(111) calculated in this work with relevant values from the literature. A calculation of initial H-abstraction from methanol is also included as a benchmark. Ethylene glycol is the only molecule of the group that has a lower barrier for initial O−H cleavage than C−H cleavage. Comparing the energy of reaction, initial C−H cleavage is near thermo-neutral or exothermic in all cases, while O−H reactions are endothermic. Further, reverse barriers (E_a-ΔE) for O−H are much lower than for C−H in all cases. While the hydrocarbon tails of the monoalcohols allow for proximity of the α-hydrogen to the metal, a rotation of the second hydroxyl away from the metal must occur for C−H scission in the case of ethylene glycol (see Figure 1B). Similarly,

Table 1. Energetics and Bond Lengths for C−H Bond-Cleaving Transition States of $C_2H_xO_2$ Dehydrogenation Intermediates of Ethylene Glycol on Pt[a]

reaction	$E_{TS} - E_o$ [eV]	ΔE [eV]	E_a [eV]	C−H [Å]	Figure 4 label
$C_2H_6O_2^* \rightarrow HOCH_2CHOH^* + H^*$	0.25	−0.36	0.79	1.54	TS1b
$HOCH_2CHOH^* \rightarrow HOCH_2COH^* + H^*$	−0.49	−0.36	0.40	1.50	TS2b
$HOCH_2CHOH^* \rightarrow HOCHCHOH^* + H^*$	−0.35	−0.49	0.54	1.60	
$HOCH_2CH_2O^* \rightarrow HOCH_2CHO^* + H^*$	0.08	−0.68	0.22	1.63	TS2c
$HOCH_2CH_2O^* \rightarrow HOCHCH_2O^* + H^*$	0.36	−0.46	0.50	1.58	TS2a
$HOCH_2COH^* \rightarrow HOCHCOH^* + H^*$	−0.61	−0.39	0.65	1.51	
$HOCHCHOH^* \rightarrow HOCHCOH^* + H^*$	−0.76	−0.27	0.62	1.58	
$HOCH_2CHO^* \rightarrow HOCH_2CO^* + H^*$	−0.18	−0.62	0.64	1.51	TS3c
$HOCH_2CHO^* \rightarrow HOCHCHO^* + H^*$	0.44	−0.09	1.26	1.71	
$HOCHCH_2O^* \rightarrow HOCCH_2O^* + H^*$	−0.20	−0.21	0.40	1.53	
$HOCHCH_2O^* \rightarrow HOCHCHO^* + H^*$	−0.60	−0.31	0.00	1.56	TS3a
$OCH_2CH_2O^* \rightarrow OCHCH_2O^* + H^*$	0.42	−0.61	0.00	1.61	
$HOCHCOH^* \rightarrow HOCCOH^* + H^*$	−0.74	−0.15	0.90	1.38	
$HOCH_2CO^* \rightarrow HOCHCO^* + H^*$	−0.69	−0.09	0.73	1.53	
$HOCCH_2O^* \rightarrow HOCCHO^* + H^*$	−0.71	−0.53	0.09	1.54	
$HOCHCHO^* \rightarrow HOCHCO^* + H^*$	−0.69	−0.82	0.23	1.57	TS4a
$HOCHCHO^* \rightarrow HOCCHO^* + H^*$	−0.67	−0.42	0.24	1.70	
$OCHCH_2O^* \rightarrow OCCH_2O^* + H^*$	0.34	−0.88	0.53	1.43	
$OCHCH_2O^* \rightarrow OCHCHO^* + H^*$	−0.19	−0.34	0.00	1.58	
$HOCHCO^* \rightarrow HOCCO^* + H^*$	−1.30	−0.36	0.43	1.61	TS5a
$HOCCHO^* \rightarrow HOCCO^* + H^*$	−1.00	−0.77	0.33	1.41	
$OCCH_2O^* \rightarrow OCCHO^* + H^*$	−0.95	−0.43	0.13	1.63	TS5b
$OCHCHO^* \rightarrow OCCHO^* + H^*$	0.08	−0.97	0.62	1.45	
$OCCHO^* \rightarrow OCCO^* + H^*$	−0.96	−0.51	0.55	1.46	TS6d

[a] $E_{TS} - E_o$ is the electronic energy of the transition state relative to that of ethylene glycol in a vacuum, a clean Pt(111) slab, and excess hydrogen atoms adsorbed on separate slabs. ΔE is the change in electronic energy of reaction (all reactants and products adsorbed on separate slabs). E_a is the activation barrier (change in electronic energy from initial state to transition state). All values are corrected for zero-point energy (ZPE). The last column shows the labels of the transition states in the Figure 4 energy diagram.

the bidentate nature of adsorbed ethylene glycol forces the C−O bonds into an angle more perpendicular to the plane of the surface than the C−O bonds in the case of monoalcohols. This facilitates proximity of the hydroxyl-hydrogen to the surface (see Figure 1C), and destabilizes the approach of the α-hydrogen to the surface, leading to a lower barrier for O−H bond scission than for C−H bond scission. The monodentate ethylene glycol binding mode consisting of only one oxygen lone pair interaction with the surface was calculated to be 0.26 eV less stable than the configuration shown in Figure 1A.

Moving to the subsequent steps of dehydrogenation, C−H bond cleavage is thermodynamically favored over O−H bond cleavage in all cases. The lowest energy transition state is for the dehydrogenation of the 1,2-dihydroxyethyl ($HOCH_2CHOH$) intermediate to the 1,2-dihydroxyvinyl ($HOCH_2COH$) intermediate. This also corresponds to the lowest barrier for dehydrogenation of $C_2H_5O_2$ species to $C_2H_4O_2$ species. For the initial C−H bond-breaking path, further dehydrogenation reaction barriers are all lower than the first reaction ($HOCH_2CH_2OH \rightarrow HOCH_2CHOH + H^*$). The O−H bond scission of the $HOCH_2CH_2O$ intermediate to form 1,2-dioxyethylene (OCH_2CH_2O) is unfavorable compared to competing C−H bond-cleaving reactions. The two potential C−H bond-cleaving reactions, to form glycolaldehyde ($HOCH_2CHO$) or $HOCHCH_2O$, have reaction barriers of 0.22 and 0.5 eV, respectively.

Among the $C_2H_4O_2$ species, the lowest energy transition state is the O−H cleavage of $HOCH_2COH$ to 2-hydroxyacetyl ($HOCH_2CO$) with a corresponding barrier of 0.24 eV. The lowest activation barriers at this level of dehydrogenation are those of C−H bond cleavage of $HOCHCH_2O$ to form HOCHCHO and of OCH_2CH_2O to form $OCHCH_2O$. Calculations show that these reactions happen with near zero barriers. In general, dehydrogenation from an alkoxide to an aldehyde carries a low energy barrier (see Table 1). Further decomposition of glycolaldehyde carries higher barriers than decomposition of $HOCHCH_2O$.

For the last three levels of dehydrogenation ($C_2H_3O_2$ through C_2HO_2), the C−C bond-breaking barriers become low enough to be competitive with dehydrogenation reactions. The lowest barrier to dehydrogenation of $C_2H_3O_2$ species to $C_2H_2O_2$ species is through the $HOCHCHO^* \rightarrow HOCHCO^* + H^*$ reaction. Interestingly, the lowest energy transition state at this level leads to the same product ($HOCHCOH^* \rightarrow HOCHCO^* + H^*$). This is not surprising given the fact that the HOCHCO intermediate is the most stable $C_2H_2O_2$ intermediate,[28] and both transition states structurally resemble the final state. The most stable transition states for the highly dehydrogenated species correspond to the $HOCCOH^* \rightarrow HOCCO^* + H^*$ and $HOCCO^* \rightarrow OCCO^* + H^*$ bond-cleaving reactions, which have energies of −1.60 and −1.71 eV relative to ethylene glycol in the gas-phase, respectively. The lowest barrier, however,

Table 2. Energetics and Bond Lengths for O−H Bond-Cleaving Transition States of $C_2H_xO_2$ Dehydrogenation Intermediates of Ethylene Glycol on Pt[a]

reaction	$E_{TS} - E_o$ [eV]	ΔE [eV]	E_a [eV]	O−H [Å]	Figure 4 label
$C_2H_6O_2^* \rightarrow HOCH_2CH_2O^* + H^*$	0.03	0.40	0.57	1.60	TS1a
$HOCH_2CHOH^* \rightarrow HOCH_2CHO^* + H^*$	−0.31	0.07	0.58	1.82	
$HOCH_2CHOH^* \rightarrow HOCHCH_2O^* + H^*$	−0.27	0.29	0.63	1.47	
$HOCH_2CH_2O^* \rightarrow OCH_2CH_2O^* + H^*$	0.63	0.56	0.77	1.50	
$HOCH_2COH^* \rightarrow HOCH_2CO^* + H^*$	−1.01	−0.19	0.24	1.35	TS3b
$HOCH_2COH^* \rightarrow HOCCH_2O^* + H^*$	−0.79	0.45	0.46	1.70	
$HOCHCHOH^* \rightarrow HOCHCHO^* + H^*$	−0.58	0.47	0.80	1.56	
$HOCH_2CHO^* \rightarrow OCHCH_2O^* + H^*$	0.22	0.63	1.05	1.83	
$HOCHCH_2O^* \rightarrow OCHCH_2O^* + H^*$	0.33	0.41	0.93	1.80	
$HOCHCOH^* \rightarrow HOCHCO^* + H^*$	−1.33	−0.09	0.33	1.38	
$HOCHCOH^* \rightarrow HOCCHO^* + H^*$	−0.86	0.31	0.79	1.34	
$HOCH_2CO^* \rightarrow OCCH_2O^* + H^*$	−0.78	0.37	0.67	1.64	TS4b
$HOCCH_2O^* \rightarrow OCCH_2O^* + H^*$	−0.81	−0.27	0.00	1.40	
$HOCHCHO^* \rightarrow OCHCHO^* + H^*$	−0.28	0.38	0.63	1.33	
$HOCCOH^* \rightarrow HOCCO^* + H^*$	−1.60	−0.30	0.20	1.34	
$HOCHCO^* \rightarrow OCCHO^* + H^*$	−1.17	0.23	0.57	1.47	
$HOCCHO^* \rightarrow OCCHO^* + H^*$	−0.96	−0.18	0.37	1.42	
$HOCCO^* \rightarrow OCCO^* + H^*$	−1.71	0.08	0.38	1.56	TS6a

[a] $E_{TS} - E_o$ is the electronic energy of the transition state relative to that of ethylene glycol in a vacuum, a clean Pt(111) slab, and excess hydrogen atoms adsorbed on separate slabs. ΔE is the change in electronic energy of reaction (all reactants and products adsorbed on separate slabs). E_a is the activation barrier (change in electronic energy from initial state to transition state). All values are corrected for zero-point energy (ZPE). The last column shows the label of the transition state in the Figure 4 energy diagram.

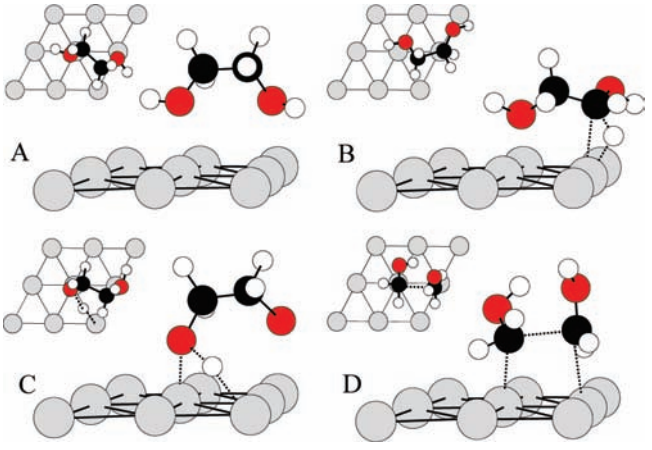

Figure 1. Schematic representations of (A) the most stable adsorption configuration of $C_2H_6O_2$, and the transition states for (B) C−H, (C) O−H, and (D) C−C bond scission of $C_2H_6O_2$ on Pt(111) calculated via DFT. Pt, carbon, oxygen and hydrogen are represented by large gray, black, red, and small white circles, respectively. For simplicity only the top layer of Pt is shown. Insets show a top view of each structure.

is for C−H bond cleavage of the $OCCH_2O$ intermediate (0.13 eV).

4.2. Carbon−Carbon Bond-Breaking Reactions in $C_2H_xO_2$ Species. Table 4 includes energetic information and transition state bond distances for C−C bond-cleaving reactions of ethylene glycol dehydrogenation intermediates. Images of all transition states and additional structural information are included in the Supporting Information.

The C−C bond cleavage of ethylene glycol on Pt(111) has a very high barrier (2.48 eV). This is not unexpected, as in order to reach the C1 products (hydroxymethyl) from the initial state, both hydroxyl branches of the molecule must rotate away from the surface to facilitate carbon-Pt bonding (see Figure 1D). The movement of the oxygen atoms away from the surface, as well as the steric hindrance of the hydrogen atoms, causes this transition state to have a relatively high energy. A similarly large barrier is seen in the C−C cleavage of 1,2-dioxyethylene (OCH_2CH_2O).

Table 3. Reaction Energy (ΔE) and Activation Barrier (E_a) for Initial Hydrogen Extraction Steps of Oxygenated Species on Pt(111)

reaction	ΔE [eV]	E_a [eV]	ref
$C_2H_6O_2^* \rightarrow HOCH_2CHOH^* + H^*$	−0.36	0.79	this work
$C_2H_6O_2^* \rightarrow HOCH_2CH_2O^* + H^*$	0.40	0.57	
$CH_3CH_2CH_2OH^* \rightarrow CH_3CH_2CHOH^* + H^*$	0.02	0.75	34[a]
$CH_3CH_2CH_2OH^* \rightarrow CH_3CH_2CH_2O^* + H^*$	0.70	0.91	
$CH_3OH^* \rightarrow CH_2OH^* + H^*$	−0.16	0.67	16
$CH_3OH^* \rightarrow CH_3O^* + H^*$	0.62	0.81	
$CH_3OH^* \rightarrow CH_2OH^* + H^*$	−0.41	0.77	this work
$CH_3OH^* \rightarrow CH_3O^* + H^*$	0.38	0.81	

[a] Information back-calculated from hydrogenation reactions.

The $C_2H_xO_2$ species derived from ethylene glycol can be split up into two segments with $-CH_xOH_y$ ($0 < x < 2, 0 < y < 1$) centers.[28] The C−C cleaving barriers can then be grouped based on the segment on both sides of the breaking C−C bond. The lowest activation barriers correspond to intermediates that are −CO terminated (η^1 (C)-acyl type bonding). Also, the lowest energy transition states for C−C bond scission are for the HOCHCO, HOCCO, and OCCO intermediates at −1.21, −1.32,

dx.doi.org/10.1021/ja201801t | J. Am. Chem. Soc. 2011, 133, 7996–8004

Table 4. Energetics and Bond Lengths for C−C Bond-Cleaving Transition States of $C_2H_xO_2$ Dehydrogenation Intermediates of Ethylene Glycol on Pt[a]

reaction	$E_{TS} - E_o$ [eV]	ΔE [eV]	E_a[eV]	C−C [Å]	Figure 4 label
$C_2H_6O_2^* \rightarrow 2CH_2OH^*$	1.94	−0.26	2.48	2.41	
$HOCH_2CHOH^* \rightarrow CH_2OH^* + CHOH^*$	0.50	−0.05	1.39	2.53	
$HOCH_2CH_2O^* \rightarrow CH_2OH^* + CH_2O^*$	0.93	−0.39	1.07	2.07	
$HOCH_2COH^* \rightarrow CH_2OH^* + COH^*$	0.08	−0.44	1.34	2.13	
$HOCHCHOH^* \rightarrow 2CHOH^*$	−0.27	0.28	1.11	2.21	
$HOCH_2CHO^* \rightarrow CH_2OH^* + HCO^*$	0.77	−0.42	1.60	2.43	
$HOCHCH_2O^* \rightarrow CHOH^* + CH_2O^*$	0.43	−0.08	1.03	2.16	
$OCH_2CH_2O^* \rightarrow 2CH_2O^*$	1.60	−0.67	1.18	2.12	
$HOCHCOH^* \rightarrow CHOH^* + COH^*$	−0.47	−0.20	1.18	2.12	
$HOCH_2CO^* \rightarrow CH2OH^* + CO^*$	−0.38	−0.77	1.07	2.53	
$HOCCH_2O^* \rightarrow COH^* + CH_2O^*$	0.33	−0.62	1.13	2.30	
$HOCHCHO^* \rightarrow CHOH^* + HCO^*$	0.05	−0.48	0.97	1.88	
$OCHCH_2O^* \rightarrow CH_2O^* + HCO^*$	0.61	−0.78	0.80	1.97	
$HOCCOH^* \rightarrow 2COH^*$	−0.68	−0.80	1.11	1.76	
$HOCHCO^* \rightarrow CHOH^* + CO^*$	−1.21	−0.63	0.52	2.13	
$HOCCHO^* \rightarrow HCO^* + COH^*$	−0.49	−0.81	0.84	1.95	
$OCCH_2O^* \rightarrow CH_2O^* + CO^*$	−0.51	−0.87	0.56	2.20	
$OCHCHO^* \rightarrow 2HCO^*$	0.05	−1.15	0.59	1.79	
$HOCCO^* \rightarrow CO^* + COH^*$	−1.32	−1.01	0.77	2.12	
$OCCHO^* \rightarrow HCO^* + CO^*$	−0.99	−1.15	0.51	1.89	TS6b
$OCCO^* \rightarrow 2CO^*$	−2.27[b]	−1.61	0.00[b]	1.63	

[a] $E_{TS} - E_o$ is the electronic energy of the transition state relative to that of ethylene glycol in a vacuum, a clean Pt(111) slab, and excess hydrogen atoms adsorbed on separate slabs. ΔE is the change in electronic energy of reaction (all reactants and products adsorbed on separate slabs). E_a is the activation barrier, (change in electronic energy from initial state to transition state). All values are corrected for zero-point energy (ZPE). [b] No clear transition state was found; however, the maximum in reaction coordinate is near the initial state.

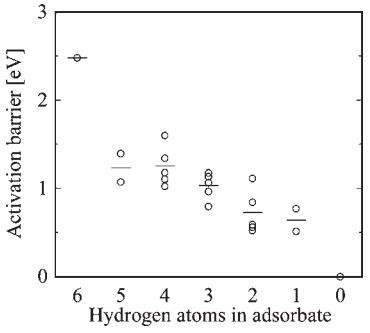

Figure 2. Carbon−carbon activation barriers of $C_2H_xO_2$ adsorbates on Pt(111) as a function of hydrogen atoms in each species. Average value of each level of dehydrogenation is denoted with a horizontal dash.

and −2.27 eV relative to ethylene glycol in the gas phase, respectively. This pattern is consistent with a previous study of C−C bond cleavage on Pt(111) that found the lowest energy transition state is ketenyl (CHCO) for ethanol dehydrogenation intermediates. Further, adsorbates with −CO branches opposite methyl and dehydrogenated methyl groups have lower barriers for C−C cleavage than other ethanol-derived adsorbates.[23]

Figure 2 shows the C−C bond-cleaving activation barriers as a function of hydrogenation of the $C_2H_xO_2$ intermediates. In terms of notation, the points aligned with '5' in the *x*-axis correspond to $HOCH_2CHOH$ and $HOCH_2CH_2O$, as each of these intermediates contains five hydrogen atoms. The average barrier for each level of hydrogenation is shown with the dash symbol. The C−C bond-breaking barriers become lower as intermediates become more dehydrogenated. The lowest calculated C−C bond-cleaving activation barriers are for the HOCHCO and the OCCHO intermediates (0.52 and 0.51 eV, respectively). The OCCO intermediate also has a very low barrier, but the exact transition state could not be located, and it appears that this intermediate decomposes spontaneously to adsorbed carbon monoxide (CO). This is an interesting finding, as it has been shown for hydrocarbons that the lowest barriers for C−C bond cleavage belong to more highly hydrogenated species.[18−21] This finding suggests that the decomposition pathway of ethylene glycol proceeds first through dehydrogenation to reach one of the species with a −CO terminus, whereupon C−C bond cleavage takes place.

5. COMPUTATION-DRIVEN EXPERIMENTS

From the DFT-calculated activation barriers, the most likely pathways for ethylene glycol decomposition on Pt in a TPD experiment can be hypothesized on the basis of reactions with the lowest activation barrier. Since the hydrogen desorption peak temperature is lower than the ethylene glycol reaction temperature, as the ethylene glycol decomposes, extracted hydrogen atoms recombine and desorb immediately. This prevents the reverse hydrogenation reactions from occurring. The DFT-predicted reaction pathway should proceed through initial O−H bond cleavage (to form $HOCH_2CH_2O$), followed by C−H bond cleavage (to form $HOCHCH_2O$ or $HOCH_2CHO$).

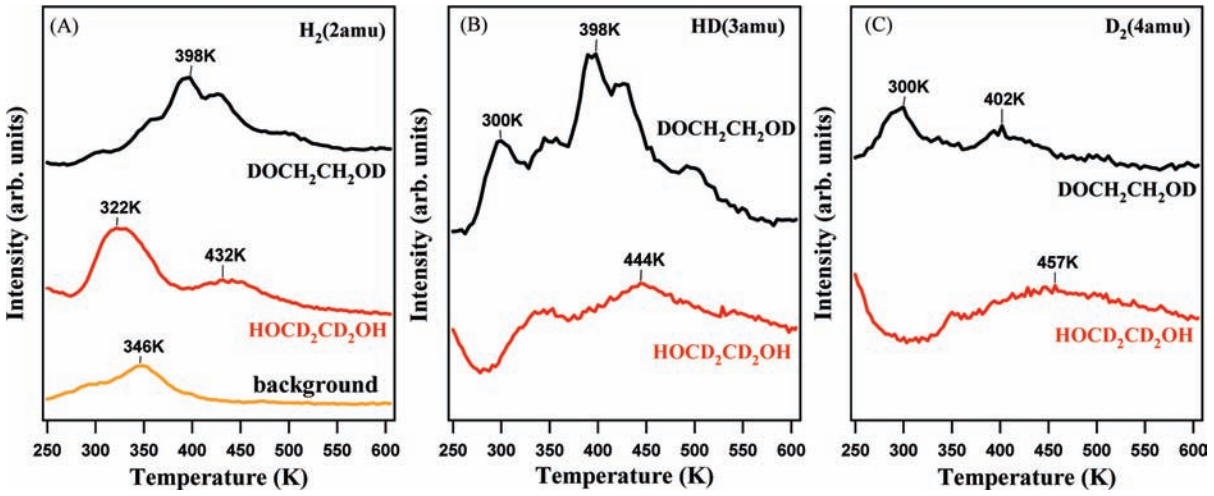

Figure 3. TPD spectra of (a) H_2, (b) HD, and (c) D_2 from the decomposition of labeled ethylene glycol ($DOCH_2CH_2OD$ and $HOCD_2CD_2OH$ shown in black and red, respectively) on the Pt(111) surface.

Calculated modified ZPE corrections based on the change in mass of deuterium-substituted intermediates and transition states indicate that kinetic isotope effects will not significantly impact relative energetics of competing reaction pathways. Given the proposed mechanism, TPD experiments with deuterated ethylene glycol ($DOCH_2CH_2OD$ or $HOCD_2CD_2OH$) were performed to assess the initial bond sequence by tracking the observed desorption temperatures of H_2, HD, and D_2 (mass 2, 3, and 4 amu, respectively) with a mass spectrometer. Fully deuterated ethylene glycol ($DOCD_2CD_2OD$) was also studied to determine the contribution from the adsorption of H_2 from the UHV background.

Figure 3 displays the TPD spectra of H_2, HD, and D_2 from deuterated ethylene glycols on the Pt(111) surface. The desorption peak of H_2 from d_2-ethylene glycol ($DOCH_2CH_2OD$) decomposition was observed at 400 K, while HD and D_2 desorbed from the surface starting at 300 K. This implies that O−D bond scission occurred before the C−H bond in d_2-ethylene glycol. It should also be noted that deuterium, in the form of HD and D_2, was also detected at higher temperatures, ~400 K, indicating that not all O−D bonds were cleaved at the lower temperature. From the d_4-ethylene glycol ($HOCD_2CD_2OH$) TPD spectra, H_2 desorbed from the surface at 330 and 450 K. The HD and D_2 desorption peaks were observed at higher temperatures (450 K) than H_2, consistent with one of the O−H bonds being broken initially followed by C−D bond scission. Overall, the TPD results of the isotopically labeled ethylene glycol are consistent with DFT predictions that the O−H bond in ethylene glycol breaks earlier than the C−H bond. At the same time, there are two desorption peaks observed for D_2 from d_2-ethylene glycol and H_2 from d_4-ethylene glycol. This implies that the two O−H bonds in ethylene glycol do not cleave at the same temperature. For example, for d_4-ethylene glycol, the peak areas of the two H_2 peaks are nearly the same after subtracting the background H_2 adsorption, providing further evidence that one of the O−H bonds breaks at ~300 K, whereas the other O−H bond cleaves at a higher temperature.

The Supporting Information contains the TPD spectra of d_2-ethylene glycol from the Ni/Pt(111) surface. In contrast to ethylene glycol TPD on Pt(111), the desorption peaks of H_2, HD, and D_2 were observed at the same temperature of 390 K on Ni/Pt(111), which was the same desorption temperature for atomic hydrogen on Ni/Pt(111). This observation suggests that the desorption of H_2 (and HD, D_2) from Ni/Pt(111) occurs after the cleavage of both the O−D and C−H bonds of ethylene glycol to produce adsorbed atomic H (and D).

Gas-phase glycolaldehyde ($HOCH_2CHO$) or glyoxal (OCHCHO) were not observed in these experiments. The DFT calculated binding energies of these two species on Pt(111) are 0.7 and 0.8 eV, respectively. Therefore, in both cases the desorption barrier is slightly higher than the activation barrier of subsequent decomposition reactions.

6. DISCUSSION

6.1. Reaction Pathways. Figure 4 shows an energy diagram of three possible decomposition pathways after initial O−H or C−H bond scission. All values shown in this figure are given with gas-phase ethylene glycol as a reference. The decomposition of ethylene glycol begins with unactivated adsorption through both hydroxyl groups. We have calculated this heat of adsorption to be 0.54 eV. The high energy of the C−C transition state (Table 4) makes it likely that initial reaction occurs through either O−H or C−H scission instead of C−C cleavage. The transition state for alkoxide formation (TS1a in Figure 4) is favorable compared to that for α-H elimination (TS1b). This is in agreement with the general observation made that alcohol decomposition on group VIII metals proceeds through an alkoxide formation.[35] Further, the desorption temperature of H_2 lower than that of HD or D_2 from the decomposition of $HOCD_2CD_2OH$ (Figure 3) indicates that the O−H bond breaks prior to C−H bonds in ethylene glycol on the Pt surface.

The further decomposition from the adsorbed 2-hydroxyethoxy ($HOCH_2CH_2O$) species requires overcoming another large barrier (TS2a or TS3c). In contrast, following the initial α-H elimination, a pathway exists that allows for lower energy transition states all the way to C1 adsorbates. Skoplyak et al. studied ethylene glycol decomposition using high resolution electron energy loss spectroscopy (HREELS) and found that the intensity of the ν(OH) mode decreases but does not

dx.doi.org/10.1021/ja201801t | J. Am. Chem. Soc. 2011, 133, 7996–8004

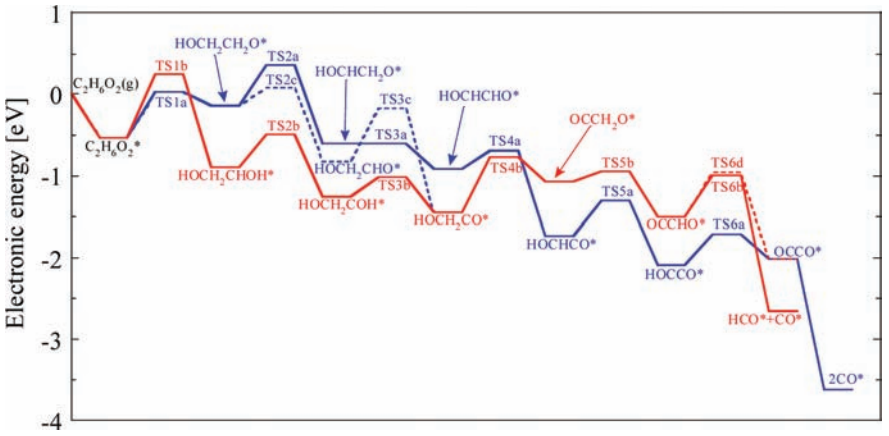

Figure 4. Energy diagram for ethylene glycol decomposition pathways on Pt(111). The red line shows the pathways through initial C−H bond scission. The blue lines show pathways from initial O−H bond scission. All values shown are with respect to gas-phase ethylene glycol, a clean Pt(111) slab, and all excess hydrogen atoms adsorbed on separate slabs. H* reaction products are omitted from labels for simplicity.

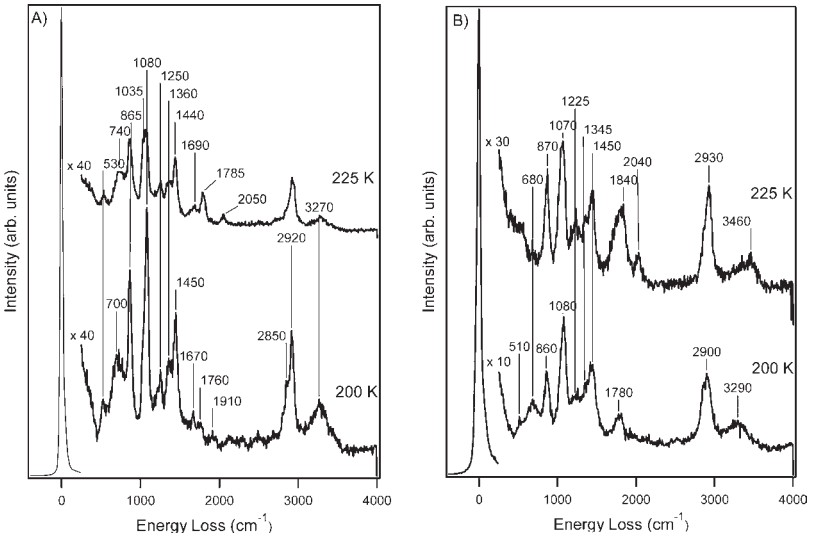

Figure 5. HREEL spectra at 200 and 225 K for thermal decomposition of ethylene glycol on (A) Pt(111) and (B) Ni/Pt(111); replotted from ref 9.

disappear when the temperature is increased from 200 to 225 K.[9] For convenience, we replot this HREELS data, along with the spectra for the Ni/Pt(111) surface in Figure 5.

Conversion of ethylene glycol to the alkoxide would explain the decrease in intensity of the ν(OH) peak, as the $HOCH_2$-CH_2O intermediate still contains a hydroxyl group bound to the surface.[28] Although this reaction explains the decrease in the ν(OH) mode, it does not explain the appearance of new modes at 1690 and 1785 cm^{-1}, which can be assigned to ν(C═C) and ν(C═O), respectively. It can be concluded from the HREELS spectrum at 225 K[9] that the surface does not contain exclusively $HOCH_2CH_2O$ or OCH_2CH_2O (as is the case for the Ni/Pt surface that is discussed in the next section). Further, the presence of higher temperature of D_2 and HD peaks from $DOCH_2CH_2OD$ decomposition and the HD peak from $HOCD_2CD_2OH$ (Figure 3) reveal that the second cleaved bond in ethylene glycol decomposition on Pt is not O−H. Combining this with the high C−C barrier computed for $HOCH_2CH_2O$ indicates that the second cleaved bond is the C−H bond. This allows us to identify path 'a' (specifically branching path 'c') in Figure 4 as the most likely reaction pathways for decomposition to C1 products on Pt.

On the basis of the calculated activation barriers for C−C bond cleavage, the four species that decompose from C2 to C1 oxygenates can most likely be identified as HOCHCO, OCCHO, HOCCO, or OCCO. Despite the low barrier for C−C bond scission through $OCCH_2O$ (0.56 eV), it is probable that this species dehydrogenates to OCCHO more readily, given the 0.13 eV barrier for C−H bond scission (shown in Figure 4). Regardless of the specific surface species through which C−C bond cleavage occurs, the proposed reaction pathways reveal that higher barriers exist for initial dehydrogenation reactions than for later C−C bond-cleaving reactions. This most likely means that the early dehydrogenation reactions are rate determining in ethylene glycol thermal decomposition on Pt. This differentiates ethylene glycol from ethane[18−21,36] and ethanol.[23] It has been concluded that rate constants for C−C bond cleavage of ethanol intermediates are higher than those for ethane intermediates.[23] An aqueous phase reforming study over Pt by Shabaker et al.

dx.doi.org/10.1021/ja201801t |J. Am. Chem. Soc. 2011, 133, 7996–8004

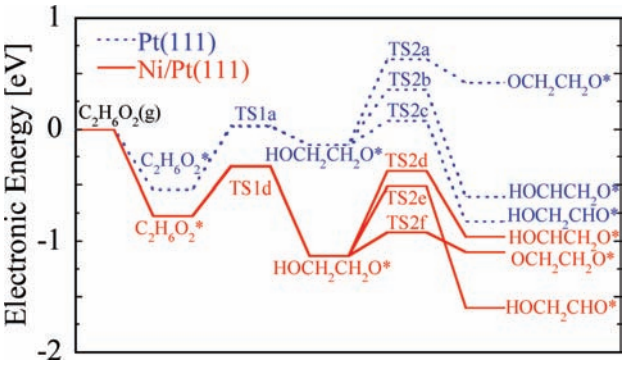

Figure 6. Energy diagram for initial dehydrogenation steps of ethylene glycol on Pt(111) (blue dotted line) and Ni/Pt(111) (red solid line). All values shown are with respect to gas-phase ethylene glycol, a clean slab, and all excess hydrogen atoms adsorbed on separate slabs. H* reaction products are omitted from labels for simplicity.

Table 5. Energy Corresponding to Figure *6* for Select Transition States and Intermediates of Ethylene Decomposition on Pt(111) and Ni/Pt(111)[a]

	relative energy [eV]	
intermediate or transition state	Pt(111)	Ni/Pt(111)
$C_2H_6O_2(g)+*$	0.00	0.00
$C_2H_6O_2*$	−0.54	−0.77
$C_2H_6O_2*\rightarrow HOCH_2CH_2O*+H*$ (TS1a,TS1d)	0.03	−0.33
$HOCH_2CH_2O*$	−0.14	−1.13
$HOCH_2CH_2O*\rightarrow OCH_2CH_2O*+H*$ (TS2a,TS2f)	0.63	−0.92
OCH_2CH_2O*	0.42	−1.10
$HOCH_2CH_2O*\rightarrow HOCHCH_2O*+H*$ (TS2b,TS2d)	0.36	−0.37
$HOCHCH_2O*$	−0.60	−0.96
$HOCH_2CH_2O*\rightarrow HOCH_2CHO*+H*$ (TS2c,TS2e)	0.36	−0.51
$HOCH_2CHO*$	−0.82	−1.60

[a] All reported values are electronic energy of the transition state relative to that of ethylene glycol in a vacuum, a clean Pt(111) or Ni/Pt(111) slab, and excess hydrogen atoms adsorbed on separate slabs. Labels in parentheses correspond to Figure 6.

gives further evidence that the decomposition rates of ethylene glycol are controlled by the initial dehydrogenation reactions. It was concluded that, due to the similarity in reaction rate orders between methanol and ethylene glycol, C−C bond breaking is most likely not rate limiting.[37] The DFT results in the current study provide an explanation for this finding, revealing that several very low activation barriers exist for C−C scission in the $C_2H_xO_2$ intermediate set.

6.2. Insights into Ni/Pt Bimetallic Catalyst Activity. As briefly mentioned in the previous section, HREELS results for ethylene glycol decomposition on Ni/Pt(111) show different decomposition progression than on Pt(111).[9] By understanding the mechanistic differences in decomposition on these surfaces, one can begin to understand the origin of observed increased activity on the Ni/Pt(111) bimetallic catalyst. Once again, DFT calculations are helpful in gaining understanding of elementary reactions. The HREELS experiments of Skoplyak et al. clearly demonstrate that on the Ni/Pt(111) surface ethylene glycol decomposes through hydrogen extraction from both hydroxyl groups to form 1,2-dioxyethylene (OCH_2CH_2O).[9] This 1,2-dioxyethylene intermediate has also been observed on Rh(111).[13] Conversely, our DFT calculations show this pathway to be energetically unfavorable on Pt(111). The OCH_2CH_2O intermediate on Pt(111) is approximately 1 and 1.2 eV less stable than the $HOCHCH_2O$ and $HOCH_2CHO$ intermediates, respectively. This is not the case for the Ni/Pt(111) surface.

Figure 6 shows the first two dehydrogenation steps resulting from initial O−H bond scission on both Pt(111) and Ni/Pt(111). Relative to ethylene glycol in the gas-phase, OCH_2CH_2O is over 1.5 eV more stable on Ni/Pt(111) than on Pt(111) (see Table 5). Also, unlike the Pt(111) surface, the barrier for formation of OCH_2CH_2O from $HOCH_2CH_2O$ on Ni/Pt (path 'f' in Figure 6) is lower than the barrier for $HOCHCH_2O$ formation (path 'd' in Figure 6) and $HOCH_2CHO$ formation (path 'e' in Figure 6). The nature of this energetic difference can be traced to the atomic binding energy of oxygen. It has been shown that the adsorbate binding energy scales linearly with the atomic binding energy of the binding atom.[38] Further, this relationship holds for bimetallic surfaces,[28] and the DFT calculated binding energy of oxygen on Ni/Pt(111) is 0.8 eV stronger than on Pt(111) (4.7 vs 3.9 eV).

The increased activity on the bimetallic surface can be linked to the lower activation barriers associated with early dehydrogenation (see Figure 6). Further, the general pathway for decomposition on the bimetallic surface is at a lower energy. A higher binding energy of ethylene glycol increases the ratio of reaction to desorption. Additionally, the energetic cost from adsorbed ethylene glycol ($C_2H_6O_2*$) to the second hydrogen extraction transition state (TS2b and TS2c) on Pt(111) is higher than on Ni/Pt(111). Since the early dehydrogenation reactions are kinetically important for ethylene glycol decomposition on Pt-based surfaces, the differences shown in Figure 6 between the activation barriers and intermediate stability on Pt(111) and Ni/Pt(111) provide a possible reason for the increased activity of the bimetallic catalyst. These fundamental insights into oxygenate activity can assist in designing active catalysts for biomass conversion to fuels and chemicals by modifying the surface to control the bond-breaking sequence.

7. CONCLUSIONS

DFT-calculated transition states of the elementary reactions involved in thermal decomposition of ethylene glycol on Pt(111) and select pathways on Ni/Pt(111) bimetallic surface were computed. Additionally, TPD experiments with deuterated ethylene glycols and HREELS results were used to assess the reaction pathways predicted computationally. For the Pt surface, it was determined that decomposition occurs through initial O−H bond cleavage to form an alkoxide intermediate ($HOCH_2CH_2O$). Next, C−H bond cleavage occurs to form the $HOCHCH_2O$ or $HOCH_2CHO$ intermediate. This bond-breaking sequence (O−H then C−H) differs from previously predicted decomposition reaction pathways of monoalcohols. Specifically, the second alcohol group in ethylene glycol alters the adsorption geometry and makes the activation of the C−H bond less favorable. A general trend was identified that barriers to C−C bond cleavage decrease as the number of hydrogen atoms in the intermediate decreases. Further, early dehydrogenation reactions are kinetically important in ethylene glycol thermal decomposition on Pt(111). C−C bond breaking probably occurs through one

or more of the following surface intermediates: HOCHCO, OCCHO, HOCCO, and/or OCCO. This finding implies that the C−C bond breaking for ethylene glycol and possible polyol biomass derivatives differs from the accepted consensus of less oxygenated alcohols[22] and hydrocarbon cracking[18−21] where C−C bond breaking is thought to be rate determining.

The energetics of the initial dehydrogenation steps on Pt show large differences from those on Ni/Pt. The low energy pathway on Ni/Pt leads to the formation of 1,2-dioxyethylene (OCH_2-CH_2O), consistent with HREELS experiments.[9] It is this favorable energetic pathway to OCH_2CH_2O that leads to increased activity on the Ni/Pt(111) surface compared to the Pt(111) surface. This observation is consistent with experimental data[1,8,9] and underscores the tunability in cleaving different bonds by surface modification, such as use of single monolayer bimetallic catalysts.

■ ASSOCIATED CONTENT

Supporting Information. Additional structural and energetic information on the DFT calculated transition states and intermediates. TPD spectra from the decomposition of d_2-ethylene glycol on Pt(111) and Ni/Pt(111). This material is available free of charge via the Internet at http://pubs.acs.org.

■ AUTHOR INFORMATION

Corresponding Author
jgchen@udel.edu; vlachos@udel.edu

■ ACKNOWLEDGMENT

This material is based upon work financially supported as part of the Catalysis Center for Energy Innovation, an Energy Frontier Research Center funded by the U.S. Department of Energy, Office of Science, Office of Basic Energy Sciences under Award Number DE-SC0001004. Additionally, DFT calculations were performed using the TeraGrid resources provided by University of Illinois' National Center for Supercomputing Applications (NCSA). We also thank Dr. Ying Chen and Dr. Orest Skoplyak for valuable discussions.

■ REFERENCES

(1) Stottlemyer, A. L.; Ren, H.; Chen, J. G. *Surf. Sci.* **2009**, *603*, 2630.
(2) Dauenhauer, P. J.; Salge, J. R.; Schmidt, L. D. *J. Catal.* **2006**, *244*, 238.
(3) Skoplyak, O.; Barteau, M. A.; Chen, J. G. *Catal. Today* **2009**, *147*, 150.
(4) Ji, N.; Zhang, T.; Zheng, M.; Wang, A.; Wang, H.; Wang, X.; Chen, J. G. *Angew. Chem., Int. Ed.* **2008**, *47*, 8321.
(5) Davda, R. R.; Shabaker, J. W.; Huber, G. W.; Cortright, R. D.; Dumesic, J. A. *Appl. Catal., B* **2005**, *56*, 171.
(6) Skoplyak, O.; Menning, C. A.; Barteau, M. A.; Chen, J. G. *Top. Catal.* **2008**, *51*, 49.
(7) Skoplyak, O.; Menning, C. A.; Barteau, M. A.; Chen, J. G. *J. Chem. Phys.* 2007, *127*, 114707.
(8) Skoplyak, O.; Barteau, M. A.; Chen, J. G. *J. Phys. Chem. B* **2006**, *110*, 1686.
(9) Skoplyak, O.; Barteau, M. A.; Chen, J. G. *Surf. Sci.* **2008**, *602*, 3578.
(10) Skoplyak, O.; Barteau, M. A.; Chen, J. G. *ChemSusChem* **2008**, *1*, 524.
(11) Huber, G. W.; Shabaker, J. W.; Evans, S. T.; Dumesic, J. A. *Appl. Catal., B* **2006**, *62*, 226.
(12) Griffin, M. B.; Jorgensen, E. L.; Medlin, J. W. *Surf. Sci.* **2010**, *604*, 1558.
(13) Brown, N. F.; Barteau, M. A. *J. Phys. Chem.* **1994**, *98*, 12737.
(14) Kandoi, S.; Greeley, J.; Sanchez-Castillo, M. A.; Evans, S. T.; Gokhale, A. A.; Dumesic, J. A.; Mavrikakis, M. *Top. Catal.* **2006**, *37*, 17.
(15) Greeley, J.; Mavrikakis, M. *J. Am. Chem. Soc.* **2002**, *124*, 7193.
(16) Greeley, J.; Mavrikakis, M. *J. Am. Chem. Soc.* **2004**, *126*, 3910.
(17) Davda, R. R.; Alcala, R.; Shabaker, J.; Huber, G.; Cortright, R. D.; Mavrikakis, M.; Dumesic, J. A. In *Science and Technology in Catalysis 2002: Proceedings of the Fourth Tokyo Conference on Advanced Catalytic Science and Technology: Tokyo, July 14-19, 2002*; Anpo, M., Onaka, M., Yamashita, H., Eds.; Elsevier: Tokyo, Kodansha, Boston, **2003**; Vol. *145*, p 79.
(18) Watwe, R. M.; Cortright, R. D.; Norskov, J. K.; Dumesic, J. A. *J. Phys. Chem. B* **2000**, *104*, 2299.
(19) Salciccioli, M.; Chen, Y.; Vlachos, D. G. *Ind. Eng. Chem. Res.* **2011**, *50*, 28.
(20) Podkolzin, S. G.; Alcala, R.; de Pablo, J. J.; Dumesic, J. A. *J. Phys. Chem. B* **2002**, *106*, 9604.
(21) Chen, Y.; Vlachos, D. G. *J. Phys. Chem. C* **2010**, *114*, 4973.
(22) Gursahani, K. I.; Alcala, R.; Cortright, R. D.; Dumesic, J. A. *Appl. Catal., A* **2001**, *222*, 369.
(23) Alcala, R.; Mavrikakis, M.; Dumesic, J. A. *J. Catal.* **2003**, *218*, 178.
(24) Soler, J. M.; Artacho, E.; Gale, J. D.; Garcia, A.; Junquera, J.; Ordejon, P.; Sanchez-Portal, D. *J. Phys.: Condens. Matter* **2002**, *14*, 2745.
(25) Ordejón, P.; Artacho, E.; Soler, J. M. *Phys. Rev. B* **1996**, *53*, 10441.
(26) Troullier, N.; Martins, J. L. *Phys. Rev. B* **1991**, *43*, 8861.
(27) Perdew, J. P.; Burke, K.; Ernzerhof, M. *Phys. Rev. Lett.* **1996**, *77*, 3865.
(28) Salciccioli, M.; Chen, Y.; Vlachos, D. G. *J. Phys. Chem. C* **2010**, *114*, 20155.
(29) Zhang, C. J.; Hu, P. *J. Am. Chem. Soc.* **2000**, *122*, 2134.
(30) Zhang, C. J.; Hu, P.; Lee, M. H. *Surf. Sci.* **1999**, *432*, 305.
(31) Alavi, A.; Hu, P. J.; Deutsch, T.; Silvestrelli, P. L.; Hutter, J. *Phys. Rev. Lett.* **1998**, *80*, 3650.
(32) ZumMallen, M. P.; Schmidt, L. D. *J. Catal.* **1996**, *161*, 230.
(33) *Avogadro: an open-source molecular builder and visualization tool*, Version 1.0.0; 2010; http://avogadro.openmolecules.net.
(34) Loffreda, D.; Delbecq, F.; Vigne, F.; Sautet, P. *Angew. Chem., Int. Ed.* **2009**, *48*, 8978.
(35) Mavrikakis, M.; Barteau, M. A. *J. Mol. Catal A: Chem.* **1998**, *131*, 135.
(36) Watwe, R. M.; Spiewak, B. E.; Cortright, R. D.; Dumesic, J. A. *J. Catal.* **1998**, *180*, 184.
(37) Shabaker, J. W.; Davda, R. R.; Huber, G. W.; Cortright, R. D.; Dumesic, J. A. *J. Catal.* **2003**, *215*, 344.
(38) Abild-Pedersen, F.; Greeley, J.; Studt, F.; Rossmeisl, J.; Munter, T. R.; Moses, P. G.; Skulason, E.; Bligaard, T.; Nørskov, J. K. *Phys. Rev. Lett.* **2007**, *99*, 016105.